

Atomic structure of the single step and dynamics of Sn adatoms on the Si(111) – $\sqrt{3} \times \sqrt{3}$ –Sn surface

R. A. Zhachuk,^{1,*} D. I. Rogilo,¹ A. S. Petrov,¹ D. V. Sheglov,¹ A. V. Latyshev,¹ S. Colonna,² and F. Ronci²

¹*Institute of Semiconductor Physics, pr. Lavrentyeva 13, Novosibirsk 630090, Russia*

²*CNR–Istituto di Struttura della Materia, via del Fosso del Cavaliere 100, I-00133 Roma, Italy*

(Dated: September 29, 2021)

The atomic structure of well-ordered single steps on the Si(111) – $\sqrt{3} \times \sqrt{3}$ –Sn surface and the dynamics of Sn adatoms in the vicinity of these steps were studied. The work was performed using low temperature scanning tunneling microscopy (LT-STM) and *ab initio* calculations based on the density functional theory. The STM tip was used to record the tunneling current *versus* time on top of oscillating adatoms, keeping the feedback loop turned off. The dynamics of adatoms, detected as the telegraph noise present in the tunneling current, was registered near the steps at 80 K. The atomic structure model of the single steps consisting of Sn atomic chains along the steps was developed. This structure leads to the formation of potential double-wells near the steps acting as traps for Sn atoms and explains the fluctuating current recorded in these areas.

PACS numbers: 68.35.Md, 68.43.Fg, 68.35.Ja

I. INTRODUCTION

Among other chemical elements used in silicon-based heterostructures for micro- and photoelectronic applications, tin attracts particular interest since it belongs to the same group as silicon and germanium. Although the Si(100) surface is a primary substrate for the fabrication of functional heterostructures based on GeSn solid solutions¹, Si(111) substrates provide a higher hole mobility for GeSn MOSFETs². However, the epitaxial growth of high-quality GeSn alloys on the Si surface is still a challenge because of the Sn surface segregation and low solubility in the Ge matrix^{1,3}. On the Si(111) surface, GeSn structures without the Sn segregation are observed after the low-temperature growth of 5 nm amorphous GeSn layer² or after the initial Sn film growth followed by the Ge deposition and substrate annealing⁴. In the second case, the Sn film starting from an even submonolayer thickness acts as a surface active agent affecting the following epitaxial growth on the Si surface^{5–8}. In particular, the surfactant Sn layer enhances the surface diffusion and suppresses the 2D island nucleation during the Ge/Si⁵ and Si/Si^{7,8} epitaxy on the Si(111) surface and prevents the Ge segregation in near-surface layers of the Si substrate⁶. This modification of the atomic processes on the growing Si(111) surface is related to the formation of Sn-induced surface reconstructions, different from the intrinsic 7×7 dimer-adatom-stacking fault structure⁹, which change the nature of the interaction between deposited atoms and the substrate. The presence of preliminarily formed Sn-induced reconstructions on the Si(111) surface also changes the orientations of the epitaxial Sn layers growing at room temperatures¹⁰. The investigation of the Sn/Si(111) surface atomic structure forming at the initial stages of Sn film growth is a way to understand how to avoid the Sn segregation at the following stages of GeSn structure fabrication.

Depending on the substrate temperature and deposited

coverage, the Sn adsorption on the Si(111)- 7×7 surface induces the formation of the following ordered surface phases^{11–13}: $\alpha - \sqrt{3} \times \sqrt{3}$ ($\sqrt{3} \times \sqrt{3}$ shortly), $\gamma - \sqrt{3} \times \sqrt{3}$ (mosaic phase) and $2\sqrt{3} \times 2\sqrt{3}$. The structure, atomic and electronic properties of these reconstructions on the Si(111) surface were well studied by the scanning tunneling microscopy (STM) technique^{12–17} and by *ab initio* calculations^{17,18}. To reveal the properties of a perfect reconstructed surface, these investigations were carried out mostly on singular regions far from surface defects and atomic steps always existing on real substrates. However, the kinetics of epitaxial growth and structural transitions on the Si(111) surface is directly determined by the features of atomic processes near the steps^{19,20} depending on the step edge orientation^{21–24}. One interesting consequence of this is the reduced symmetry island growth on the higher symmetry substrate demonstrated in case of the Si and Ge epitaxy on the Si(111) – $\sqrt{3} \times \sqrt{3}$ –Bi surface²¹. In the present work, we used STM and *ab initio* calculations based on the density functional theory to reveal the atomic structure of the steps on the Si(111) – $\sqrt{3} \times \sqrt{3}$ –Sn surface and to study the dynamics of adsorbed atoms in the vicinity of such steps.

The paper is organized as follows: after reviewing the experimental and calculation procedures, we report on the atomic structure model of the single step on the Si(111) – $\sqrt{3} \times \sqrt{3}$ –Sn surface, give corresponding experimental and calculated STM images and show the localization of empty and filled electronic states near the steps. In Sec. 4.2 we first review the previous results related to the Sn adatom dynamics on the flat (111) – $\sqrt{3} \times \sqrt{3}$ –Sn surface regions of Si and Ge. Then we report the STM data related to the adatom dynamics on the stepped Si(111) – $\sqrt{3} \times \sqrt{3}$ –Sn surface, calculate the potential energy surfaces (PES) for Sn and Si adatoms, compare the experimental and calculated data, and explain the fluctuating current detected near the steps.

II. METHODS

A. Experimental procedure

The experiments were carried out using an ultra-high vacuum system (base pressure 1×10^{-10} mbar) equipped with a low temperature scanning tunneling microscope (LT-STM, Omicron) and a low energy electron diffraction (LEED). Silicon substrates were cut from Si(111) n-type wafers with resistivity $4 \text{ m}\Omega \cdot \text{cm}$. The sample preparation started from clean Si(111) surfaces. The Si(111) $- 7 \times 7$ clean surface was prepared by the annealing at 900°C and flashing the sample at 1250°C for about 1 min. The samples were resistively heated by a direct current. The 7×7 surface reconstruction was confirmed by LEED and STM before the Sn evaporation. Sn was evaporated from a Knudsen effusion cell. The effusion cell was thoroughly outgassed before its use in order to maintain the pressure in the 10^{-10} mbar range during the metal deposition. The evaporation rate was measured by using the quartz crystal thickness monitor. A nominal $1/3$ monolayer Sn deposition was performed at room temperature, followed by the sample annealing at 650°C . After that the formation of the $\alpha - \sqrt{3} \times \sqrt{3}$ -Sn reconstruction was confirmed by LEED and STM. Electrochemically etched tungsten STM tips were used after a cleaning procedure by electron bombardment. The reported STM images were recorded at 80 K in the constant-current mode. The STM scanner was calibrated by using the Si(111) $- 7 \times 7$ surface as a reference.

Tunneling current vs time traces (“current traces” hereafter) were acquired concomitantly to the acquisition of constant current STM images by interrupting the tip scan every five points and five lines over the chosen area. At every single grid point, the STM feedback loop was switched off and the tunneling current was recorded with a sampling rate of 33 kHz. In this way, we could observe steps in the current trace if an adatom underneath the STM tip is unstable, i.e. moves horizontally or vertically. Furthermore, it is possible to exactly locate the position of moving adatoms on the STM images. To show where such traces were recorded on the sample surface, we calculated the standard deviation (σ) of all the current traces and reported these values on the z axis of a grid. The resulting images (hereinafter called “ σ maps”) show a brighter color for higher σ values, evidencing where the adatom movement occurs. It is important to emphasize that, with such an acquisition method, the uncertainties of the actual tip location during the current trace acquisition are greatly reduced because the STM image and the current traces are acquired concomitantly. The maximum limit of the detectable frequency in the current traces in our STM system is estimated to be ≈ 5 kHz, while the lower limit is about 100 Hz. The method was successfully applied to the study of Sn atom dynamics on flat Si(111) $- \sqrt{3} \times \sqrt{3}$ -Sn and Ge(111) $- \sqrt{3} \times \sqrt{3}$ -Sn surfaces at low temperatures^{25,26} and was described in detail in Ref. 27.

B. Computational details

The calculations were carried out using the pseudopotential²⁸ density functional theory SIESTA code²⁹ within generalized gradient approximation (GGA) to the exchange and correlation interactions between electrons³⁰. We did not consider the corrections to GGA, which could help to better describe the electron correlation effects in the Si(111) $- \sqrt{3} \times \sqrt{3}$ -Sn system. Such corrections, although having some influence on the calculated electronic structure^{31–34}, are expected to have a small impact on the calculated total energies and forces, and the resulting atomic structure, studied in this work. The valence states were expressed as linear combinations of the Sankey-Niklewski-type numerical atomic orbitals²⁹. In the present calculations, the polarized double- ζ functions were assigned for all atom species. This means two sets of s - and p -orbitals plus one set of d -orbitals on silicon and tin atoms, and two sets of s -orbitals plus a set of p -orbitals on hydrogen atoms. The electron density and potential terms were calculated on a real space grid with the spacing equivalent to a plane-wave cut-off of 200 Ry.

In our calculations we used (111)-slabs with single steps in the $[11\bar{2}]$ step-down direction ($[11\bar{2}]$ -steps in short). The dangling bonds at the slabs bottom side were saturated by H atoms, while the top (111)-terraces were constructed according to the $\sqrt{3} \times \sqrt{3}$ -Sn atomic model consisting of Sn-adatoms on T_4 -sites¹². The slab thickness was about 14 Å (four Si-bilayers), and the 26 Å thick vacuum layer was used. The positions of all slab atoms (except for the Si atoms in the bottom bilayer and all H atoms) were fully optimized until the atomic forces became less than 0.01 eV/Å. Two different calculation cells were used in this work. For the calculation of relative formation energies and PES maps, we used slabs with $11.6 \times 18.2 \text{ \AA}^2$ lateral dimensions and a grid of $4 \times 3 \times 1$ \mathbf{k} -points in the Brillouin zone³⁵. Larger slabs with $11.6 \times 58.4 \text{ \AA}^2$ lateral dimensions and a grid of $4 \times 1 \times 1$ \mathbf{k} -points were used for the calculation of STM images. Si and Sn chemical potentials were calculated using bulk unit cells and $10 \times 10 \times 10$ \mathbf{k} -point grids. The Sn chemical potential was calculated using the bulk α -phase of Sn having the diamond structure and known as gray tin. The calculated Si and Sn bulk-lattice constants are $a_{Si} = 5.50 \text{ \AA}$ and $a_{Sn} = 6.73 \text{ \AA}$, which are close to experimental values $a_{Si} = 5.43 \text{ \AA}$ and $a_{Sn} = 6.46 \text{ \AA}$, respectively. The constant-current STM images were produced based on the Tersoff-Hamann approximation³⁶ using the eigenvalues and eigenfunctions of the Kohn-Sham equation³⁷ for a relaxed atomic structure. Experimental and calculated STM images were processed using the WSXM software³⁸.

In this work, we compared the relative formation energies of the stepped Si(111) $- \sqrt{3} \times \sqrt{3}$ -Sn surface according to different atomic configurations of the step edge. The Si(111) $- \sqrt{3} \times \sqrt{3}$ -Sn surface having an unreconstructed step edge (described in the text) after the

structure relaxation was treated as a reference surface. The relative surface formation energies (per unit area) were calculated according to the procedure described in Ref. 39:

$$\Delta\gamma = (E_{model} - E_{unrec} - \mu_{Si}\Delta N_{Si} - \mu_{Sn}\Delta N_{Sn})/S, \quad (1)$$

where S is the unit cell area of the slab in the xy plane, E_{unrec} refers to the total energy of the reference slab containing the unreconstructed step after the structure relaxation, E_{model} is the total energy of the slab according to the trial step model, ΔN_{Si} and ΔN_{Sn} account for the number of Si and Sn atoms in the trial model in excess of those in the reference model.

μ_{Si} and μ_{Sn} are the chemical potentials of Si and Sn, which are the energy per atom in the reservoirs with which the surface is assumed to be in equilibrium. Since the surface is in equilibrium with the bulk Si substrate, μ_{Si} is the energy per atom in bulk Si. The adsorbate chemical potential μ_{Sn} was treated as a variable, since its exact value is unknown. It corresponds to a real physical variable that can be externally tuned³⁹. Under thermodynamic equilibrium conditions the surface having the lowest formation energy will be realized. The change of μ_{Sn} leads to a change of surface formation energy, which may be followed by structural phase transitions. The chemical potential in bulk α -phase Sn ($\mu_{Sn-bulk}$) may be considered as the upper bound for the Sn chemical potential. If $\mu_{Sn} > \mu_{Sn-bulk}$, then bulk α -phase Sn would be energetically more favorable than any adsorbed phase, which would lead to the precipitation of bulk Sn on the Si surface. In the opposite case of extreme low μ_{Sn} values, the clean Si surface with no Sn adatoms becomes the most stable. Thus, the low/high μ_{Sn} values should favor atomic structures with a low/high amount of Sn atoms on the Si surface, respectively. In this work we are interested in the intermediate μ_{Sn} values, when the Sn-Si compound surface phases are stable.

The PES maps describing the energetics of adatoms on the stepped $\text{Si}(111) - \sqrt{3} \times \sqrt{3}$ -Sn surface were produced for the positions of the adsorbed probe Sn (Si) atom within a symmetry-irreducible half of the calculation cell. For each xy -coordinate, the adsorbed atom was initially placed approximately 3 Å above the surface and its z -coordinate was allowed to relax, while the coordinates in the xy -plane were kept fixed. The positions of all remaining atoms, but the bottom Si-H units, were fully optimized until atomic forces became less than 0.01 eV/Å. The total of 444 points forming a grid with about 0.5 Å spacing were calculated in the calculation cell half. The PES data for the whole calculation cell were recovered by applying the mirror symmetry transformation to the calculated PES data. The exact energies of local energy minima on PES were calculated with a free-moving probe atom placed near the local energy minima.

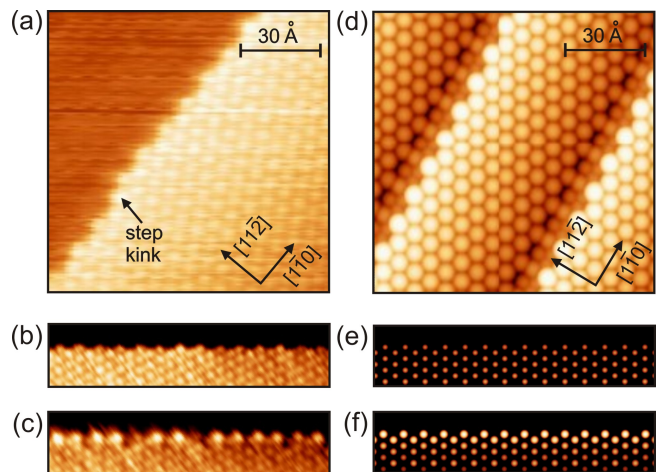


Figure 1. Experimental (a), (b), (c) and calculated (d), (e), (f) constant-current STM images of single steps on the $\text{Si}(111) - \sqrt{3} \times \sqrt{3}$ -Sn surface. (a), (b), (d), (e) $U = +1.0$ V, (c), (f) $U = -1.0$ V. The calculated STM images are based on the “B” atomic model of the single step on the $\text{Si}(111) - \sqrt{3} \times \sqrt{3}$ -Sn surface (see the text).

III. RESULTS AND DISCUSSION

A. Atomic structures of the single step on the $\text{Si}(111) - \sqrt{3} \times \sqrt{3}$ -Sn surface

The starting point of our investigation of the step atomic structure is the information provided by STM images. In Fig. 1(a) is a typical STM-image of the atomic step found on the $\text{Si}(111) - \sqrt{3} \times \sqrt{3}$ -Sn surface. Each bright spot in the STM image represents a Sn adatom. In Figs. 1(b) and 1(c) are the high-resolution STM-images of the step edge obtained at $U = +1.0$ V and $U = -1.0$ V, respectively. It is seen in Fig. 1(c) that the Sn adatoms at the upper terrace edge look brighter than those far from it at $U = -1.0$ V. Since this effect was observed only at a negative bias, then it is unlikely that it is a real topography feature. The effect is most probably due to a charge transfer and associated higher density of filled local electron states (electrons) at the Sn atoms located at the upper terrace edge.

In Fig. 2(a) is the experimental STM image of the single step on the $\text{Si}(111) - \sqrt{3} \times \sqrt{3}$ -Sn surface acquired at $U = -1.0$ V after a linear distortion correction and an FFT band pass filtering. The key for understanding the step edge directions is in the mutual alignment of the $\sqrt{3} \times \sqrt{3}$ -Sn lattices on the neighboring (111) terraces separated by the single step. Accordingly, the hexagonal lattice was drawn across the Sn adatom positions on the upper terrace (lower right part of Fig. 2(a)). It is clear that the Sn adatoms on the lower terrace (upper left part of Fig. 2(a)) are located on the same lines drawn perpendicular to the step edge as the Sn adatoms on the upper terrace. Two (the only possible) models of unreconstructed steps on the $\text{Si}(111) - \sqrt{3} \times \sqrt{3}$ -Sn sur-

face compatible with the above observation are shown in Figs. 2(b) and 2(c). Thus, the direction along the step edge in Figs. 1(a) and 2(a) is of $[\bar{1}\bar{1}0]$ -type, as it follows from the models shown in Figs. 2(b) and 2(c).

A more difficult question is the step-down direction in the experimental STM images shown in Figs. 1(a) and 2(a). This direction can be either $[\bar{1}\bar{1}2]$, resulting in a step in which the bonds configuration is the same as on unreconstructed (001) surface (right parts of Figs. 2(b) and 2(c)) or $[\bar{1}1\bar{2}]$, in which the bonds configuration is as on the (110) surface (left parts of Figs. 2(b) and 2(c)). It should be noted that these two directions are physically nonequivalent for crystals with a diamond lattice, i.e. they lead to a different step atomic structure with different properties. To solve this problem, we note that the bright spots (Sn atoms) on the lower terrace shown in Fig. 2(a) are shifted from the nearest nodes of the hexagonal lattice by about $1/3$ lattice period (≈ 2.2 Å) towards the step edge. The shift is clearly visible near the central part of the lower terrace. The Sn atom positions on the lower terrace near the step edge should be ignored since, in this area, the image may be altered by an undesired tunneling through the side of the STM tip. The same shift direction can be observed only for $[\bar{1}1\bar{2}]$ steps. Therefore, the steps observed in our experimental STM images in Figs. 1(a) and 2(a) are $[\bar{1}1\bar{2}]$ steps.

The trial atomic models of the steps for *ab initio* calculations were constructed in accordance with the information provided by experimental STM images. In this work, we compare the stability of different step configurations by calculating the relative formation energies of regular stepped surfaces according to various step models. The step formation energies were not calculated explicitly.

We performed an extensive search for the lowest energy atomic configuration of the stepped $\text{Si}(111) - \sqrt{3} \times \sqrt{3} - \text{Sn}$ surface. 50 atomic models were evaluated, and our results are shown in Fig. 3. Three solid lines - red, black, and blue - represent the surface energy graphs for three lowest energy atomic configurations, A, B, and C, depending on the μ_{Sn} value, while the dashed lines in Fig. 3 are from other higher energy trial models.

The atomic step model “B”, which is stable in a wide range of μ_{Sn} values (Fig. 3) is shown in Fig. 4. The difference between this model and the model of unreconstructed step shown in Figs. 2(b) and 2(c) (left parts of these figures) is the presence of Sn atomic chain consisting of A_1 and A_2 Sn adatoms decorating the step edge. The adatom A_1 can be considered as the one taken from the $\sqrt{3} \times \sqrt{3} - \text{Sn}$ structure on the lower terrace by shifting from the neighboring T_4 site to the step edge (see the dashed circle outlining the previous position of this adatom). The adatom A_2 is an additional Sn atom, not existing in the unreconstructed step model. The model “B” contains Si atoms with unsaturated dangling bonds (rest atoms): R_1 on the upper terrace and R_2 on the lower terrace. The rest atoms show the sp^2 -like (planar) configuration of saturated bonds after the structure relaxation. While R_1 exists also in the unreconstructed step model,

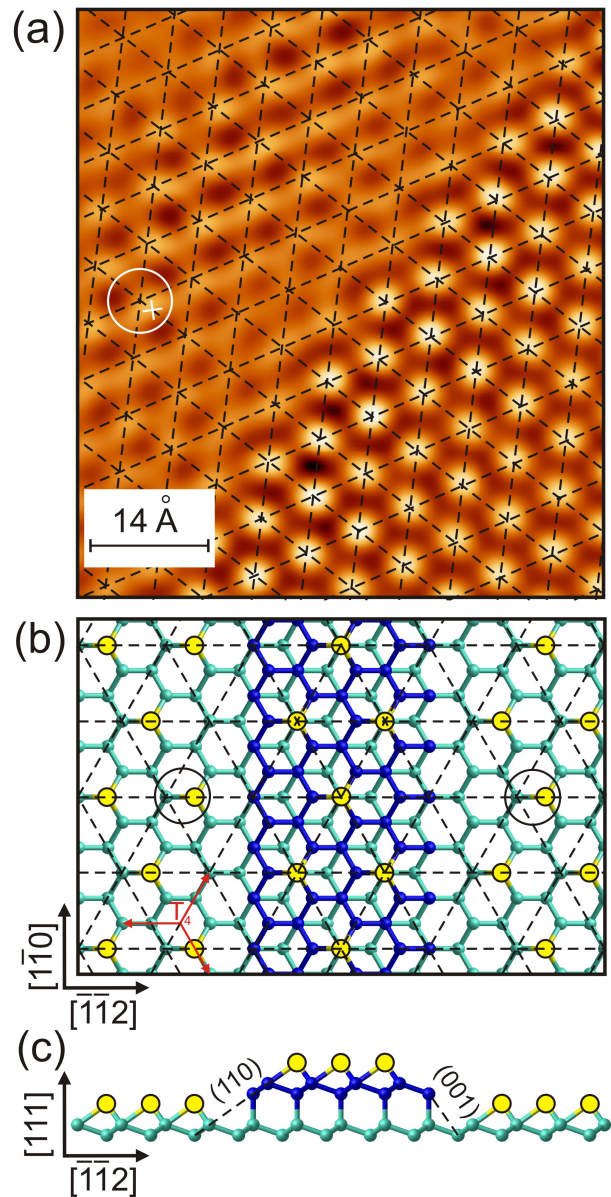


Figure 2. (a) Experimental STM image of the step on the $\text{Si}(111) - \sqrt{3} \times \sqrt{3} - \text{Sn}$ surface after FFT band pass filtering, $U = -1.0$ V. The image was carefully corrected for the minimal distortion using the hexagonal lattice of the upper terrace (lower right part of the image) as a reference. The white cross marks the position of bright spot on the lower terrace. (b), (c) Atomic models of unreconstructed steps on the $\text{Si}(111) - \sqrt{3} \times \sqrt{3} - \text{Sn}$ surface with $[\bar{1}1\bar{2}]$ and $[\bar{1}\bar{1}2]$ steps (left and right step, respectively). Cyan and blue circles are Si atoms of the lower and upper (111) terraces, respectively, yellow circles are Sn adatoms. The hexagonal lattices (dashed lines) in (a) and (b) are drawn across the positions of Sn adatoms on the upper terrace, while large circles highlight the deviations of the lattice nodes from the nearest Sn positions.

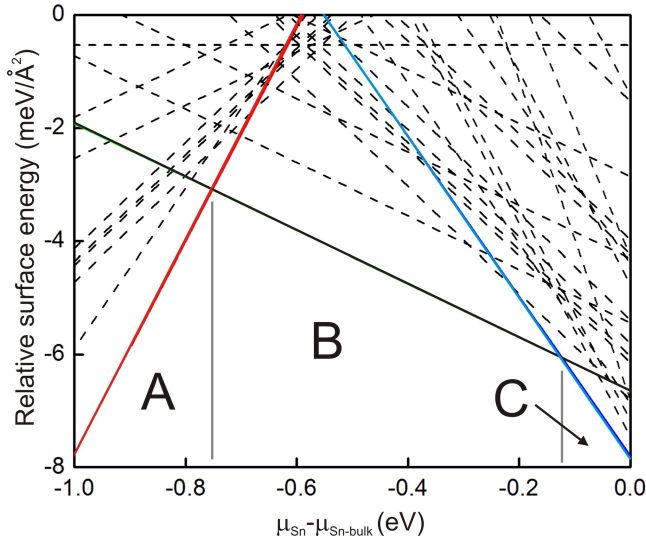


Figure 3. Surface-energy diagram of the stepped $\text{Si}(111) - \sqrt{3} \times \sqrt{3}$ -Sn surface. The energies are given relative to the formation energy of relaxed surface with unreconstructed steps (see the text) for the Sn adsorbate. The models marked as “A” (red solid line), “B” (black solid line), and “C” (blue solid line) correspond to the lowest-energy surface atomic configurations found for $-1.0 \text{ eV} < \mu_{\text{Sn}} - \mu_{\text{Sn-bulk}} < 0.0 \text{ eV}$. Black dashed lines are from other trial models.

the emergence of R_2 is caused by the Sn atom shift leading to the formation of A_1 step edge atom. All other Si bonds in the model, except for the bonds on R_1 and R_2 atoms, are saturated. It is difficult to resolve A_1, A_2, R_1 and R_2 atoms experimentally since Sn adatoms, in the vicinity of the upper terrace edge, strongly hinder their imaging. The possible reason of why Sn atoms prefer A_1 and A_2 positions at the step edges is the bigger size of Sn atoms, as compared to that of Si. As a result, Sn atoms better fit the positions with large distances to the closest neighbors, as it is the case for A_1 and A_2 .

Model “C” is stable at the excess of Sn on Si surface, just before precipitation of the bulk Sn (Fig. 3). The only difference between “B” and “C” models is that, in case of the “C” model, the Si rest atom R_2 is substituted with the Sn atom. Both models result in very similar calculated STM images. Model “A” is stable at low μ_{Sn} values and contains no Sn atoms at all. This clean Si surface model is basically the unreconstructed step edge model shown in Figs. 2(b) and 2(c) (left parts) where all Sn atoms on (111) terraces are substituted by Si atoms. Thus, the terraces in model “A” are structurally similar to the mosaic $\sqrt{3} \times \sqrt{3}$ -Sn γ -phase observed after the partial self-cleaning of $\text{Si}(111)$ terraces at elevated temperatures^{11,13}. The models “A” and “C” determine the upper and lower stability boundaries of the “B” model, which is most likely to be relevant for the experimentally observed step structure.

In Fig. 1(d) is a large-scale calculated STM image of the $\text{Si}(111) - \sqrt{3} \times \sqrt{3}$ -Sn surface based on the atomic

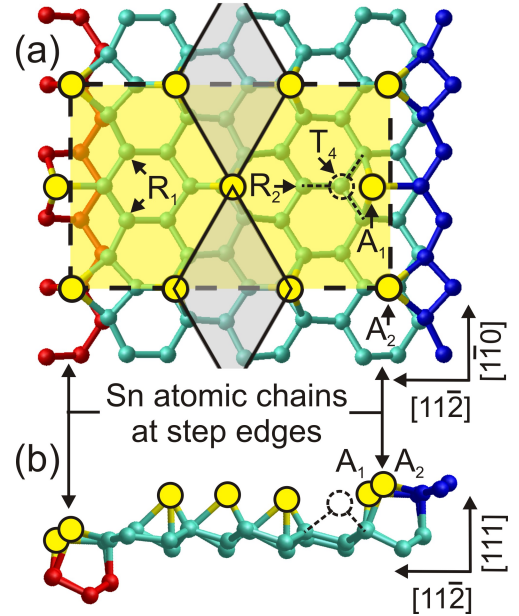


Figure 4. Atomic model “B” of the step edge on the $\text{Si}(111) - \sqrt{3} \times \sqrt{3}$ -Sn surface. Red, cyan, and blue circles are Si atoms of the lower, middle and upper (111) terraces respectively, yellow circles are Sn adatoms. Gray shaded rhombuses are the unit cells of the $\sqrt{3} \times \sqrt{3}$ -Sn reconstruction, the yellow shaded rectangle outlined by dashed line is the calculation unit cell. A_1 and A_2 denote Sn adatoms at the step edges forming Sn atomic chains, R_1 and R_2 are the Si rest atoms. The site outlined by a dashed circle and marked as T_4 shows the place where the A_1 atom came from. (a) Top view. (b) Side view.

step model “B” shown in Fig. 4. In Figs. 1(e) and 1(f) are the STM images of the step edges calculated for $U = +1.0 \text{ V}$ and $U = -1.0 \text{ V}$, respectively. The latter two images exhibit the same features as the experimental STM images shown in Figs. 1(b) and 1(c): namely, the spots associated with Sn adatoms at the very edge of the upper terrace are brighter than other spots on the filled states STM images ($U < 0$). This effect was not observed at $U = +1.0 \text{ V}$ in agreement with the experimental data (Figs. 1(b) and 1(e)). Thus, the experimental and calculated STM images demonstrate a good match, which is a prerequisite for a correct atomic model. It should be noted that few other trial models exhibited the same effect of bright terrace edges as the model shown in Fig. 4, but these atomic configurations had significantly higher formation energies.

The charge distribution near the step edge is the reason for the increased intensity on Sn adatoms in the filled states experimental and calculated STM images. This effect was investigated in more detail. The calculated local density of states (LDOS) isosurfaces integrated in a 1.0 eV energy window below and above the calculated Fermi level are shown in Fig. 5. The atomic model superimposed on this pattern allows identifying the atoms

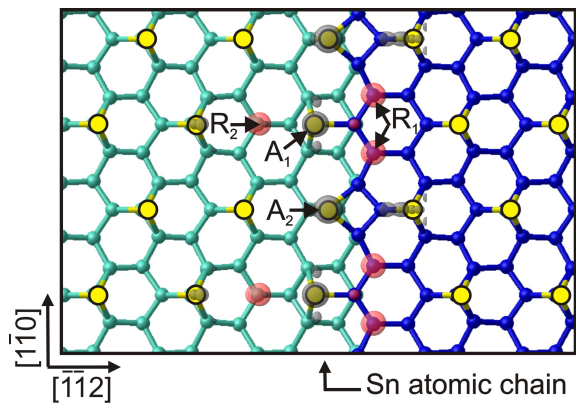


Figure 5. LDOS isosurfaces integrated in a 1.0 eV energy window below (half-transparent gray areas) and above (half-transparent red areas) the calculated Fermi level. The atomic model “B” of the Si(111) - $\sqrt{3} \times \sqrt{3}$ -Sn stepped surface is overlaid. Cyan and blue circles are Si atoms of the lower and upper (111) terraces, respectively, yellow circles are Sn adatoms. A_1 and A_2 denote Sn adatoms at the step edge forming the Sn atomic chain, R_1 and R_2 are the Si rest atoms on the upper and lower (111) terraces, respectively.

acting as electron donors or acceptors. It is clear that the empty states are mostly concentrated on the Si rest atoms, while filled states are mostly located on A_1 and A_2 atoms of the Sn chain. Few filled states are also found on the Sn atoms near the lower and upper terrace edges.

B. PES and dynamics of Sn adatoms on the Si(111) - $\sqrt{3} \times \sqrt{3}$ -Sn surface with steps

The dynamical fluctuations of Sn atoms on flat Sn/Si(111) and Sn/Ge(111) surfaces were studied in detail in Refs. 25 and 26 by recording the tunneling current as a function of time. Vertical fluctuations of Sn atoms within the $\sqrt{3} \times \sqrt{3}$ surface reconstruction are related to the $\sqrt{3} \times \sqrt{3} \rightarrow 3 \times 3$ phase transition during the temperature decrease. The process is well described within the dynamical fluctuations model, at least in case of the Sn/Ge(111) system. According to this model, the static $\sqrt{3} \times \sqrt{3}$ structure is unstable and transforms into the 3×3 structure with the Sn adatoms buckled up and down⁴⁰. The observation of the $\sqrt{3} \times \sqrt{3}$ structure, according to this theory, is due to the time averaged vertical fluctuations of Sn atoms, which is 0.36 Å between the up-and-down positions on Sn/Ge(111)⁴¹. The fluctuations were observed at 80 – 220 K in the Sn/Ge(111) system and at 2.3 – 32 K in the Sn/Si(111) system. While the stable 3×3 structure was actually observed in the Sn/Ge(111) system at 80 K, the $\sqrt{3} \times \sqrt{3}$ reconstruction on Sn/Si(111) persists even at a very low temperature, down to 2.3 K²⁷. The reason for that is a very low energy barrier (2.6 ± 1.4 meV²⁶) associated with the phase transition on Sn/Si(111), which is much lower than that on Sn/Ge(111) (13 ± 7 meV²⁵). This results in the no-

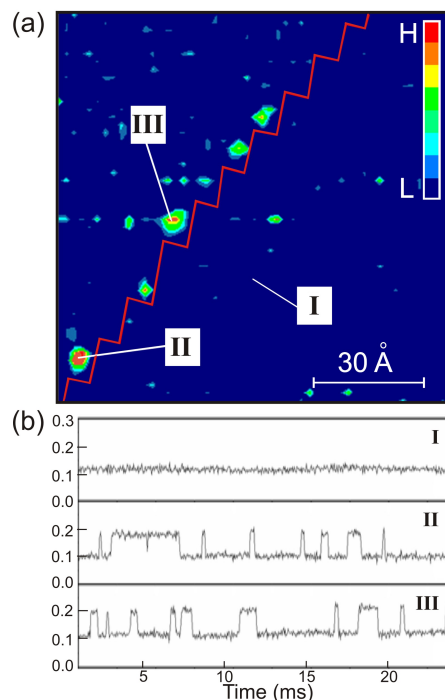


Figure 6. (a) σ map related to the constant-current STM image shown in Fig. 1(a). The location of the step edge in the STM image is indicated by a red line. (b) A collection of current traces detected on the flagged surface spots.

table quantum tunneling of Sn adatoms between two stable positions on Sn/Si(111) and that destroys the 3×3 structural order²⁶.

Due to the very low energy barrier in the Sn/Si(111) system, the frequency of Sn dynamical fluctuations at 80 K is expected to be well above the maximum limit of detectable frequency in our STM measurements (about 5 kHz). It is possible to estimate how high the energy barriers have to be in order to observe the dynamical fluctuations in STM. To this end, we make use of the frequency (f) of thermally activated dynamical fluctuations using an Arrhenius relation $f = f_0 \exp(-E_a/kT)$, where k , T , and f_0 stand for the Boltzmann constant, sample temperature and attempt frequency, respectively, which can be approximated by the Debye frequency of Si (14 THz). Thus, for the upper limit of detectable frequency (5 kHz), we get $E_a = 0.13$ eV and for the lower limit (100 Hz) - $E_a = 0.15$ eV.

Figure 6(a) shows the σ map acquired concomitantly with the STM image shown in 1(a). All the current traces recorded on the terrace show a flat profile ($\sigma \approx 0$) consistent with the expected high frequency of Sn dynamical fluctuations at 80 K (see the current trace collected at point I, for example). However, the σ map clearly exhibits bright spots at the lower side of step edge, that show the presence of current traces with a high standard deviation value. As an example, two stepped current traces collected at points II and III are reported in Fig. 6(b). The observation of stepped current traces near

Table I. Relative energies (eV) of local energy minima on PES for the adsorbed Sn and Si probe atoms on the stepped $\text{Si}(111) - \sqrt{3} \times \sqrt{3} - \text{Sn}$ surface. N is the local minimum number according to Fig. 7.

N	Relative energy (eV)	
	Sn	Si
1	0	0
2	-0.33	-0.48
3	-0.58	-0.55
4	-0.28	-0.61
5	-0.19	-0.51
6	-0.07	-0.23
7	-0.37	-0.52
8	-0.49	-0.68
9	-0.39	-0.47
10	-0.18	-0.23

the step edge at 80 K indicates that the energy barrier for the fluctuating adatoms in that area is much larger than that on the flat Sn/Si(111) surface. It is also worth noting that, in spite of a very regular step structure visible in the STM image in Fig. 1(a), only a few irregular spots are visible in the σ map in Fig. 6(a). The reason for that will be clear from the results presented below.

The calculated PES for a Sn probe atom on the stepped $\text{Si}(111) - \sqrt{3} \times \sqrt{3} - \text{Sn}$ surface with the atomic model “B” overlaid is shown in Fig. 7. Bright regions correspond to the energy minima, while dark regions indicate energy maxima. It is clear that the Sn adatom positions on the surface are the highest energy maxima on PES. This is because these atoms have only one dangling bond and, therefore, these sites are not favorable for the adsorption of additional probe Sn atom having four valence electrons. The positions of rest atoms also show energy maxima, but their values are lower than those found on Sn atoms.

All Si bonds on the $\text{Si}(111) - \sqrt{3} \times \sqrt{3} - \text{Sn}$ surface are saturated by Sn atoms making this surface inert. Thus, according to Fig. 7, each $\sqrt{3} \times \sqrt{3} - \text{Sn}$ half unit cell shows only a single shallow local minimum on T_4 site (minimum $N = 1$). The energy of this local minimum is taken as the energy zero in our calculations. The energies calculated for different energy minima on PES for Sn and Si probe atoms are shown in Tab. I. As expected, the deepest minima are located near the step edge since this area contains many unsaturated bonds. According to Fig. 7, each rest atom is surrounded by four local minima on PES: $N = 2, 2, 3, 3$ for R_2 and $N = 7, 8, 9, 10$ for R_1 . The region between A_1 and A_2 adatoms contains three additional minima: $N = 4, 5, 6$. The location of the deep local minima around rest atoms and near adatoms is typical of the surfaces containing these atoms, and it was also observed in other systems^{42,43}. The reason for this is that the adsorbed atom in the vicinity of rest atoms and adatoms may effectively saturate several bonds. Ac-

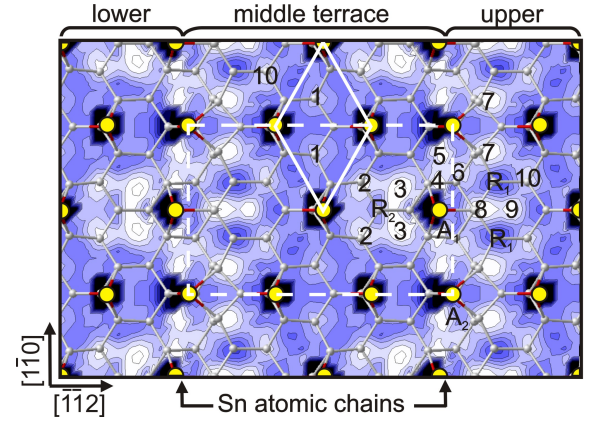


Figure 7. PES of an adsorbed Sn probe atom on a stepped $\text{Si}(111) - \sqrt{3} \times \sqrt{3} - \text{Sn}$ surface; the atomic model “B” is overlaid. The contour spacing is 0.2 eV. Bright (dark) regions indicate energy minima (maxima). Numbers indicate different local minima on PES. White circles are Si atoms, yellow circles are Sn atoms. A_1 and A_2 denote Sn atoms at the step edges forming Sn atomic chains, R_1 and R_2 are the Si rest-atoms on (111) terraces. The rectangle outlined by a white dashed line is the calculation unit cell of the stepped surface, the rhombus outlined by a white solid line is the $\sqrt{3} \times \sqrt{3} - \text{Sn}$ unit cell on the (111) terrace.

ording to Tab. I, the two neighboring minima near R_2 labeled $N = 3$ on PES are the deepest (global) minima for the probe Sn atom on the stepped $\text{Si}(111) - \sqrt{3} \times \sqrt{3} - \text{Sn}$ surface. Therefore, these minima should be the preferential adsorption sites for Sn atoms at a low sample temperature.

The calculated PES (Fig. 7) shows that the energy barrier between two neighboring $N = 3$ sites is among the lowest on the surface. As it follows from the symmetry of the computational cell, the saddle point between these two sites is situated in the $(1\bar{1}0)$ plane crossing A_1 atom. The total energy related to this saddle point was calculated by relaxing the atomic structure while restricting the Sn probe atom movement to the $(1\bar{1}0)$ plane. It was found that the energy barrier between two neighboring $N = 3$ sites is as low as 0.21 eV. Thus, these two global minima sites are separated by a low energy barrier and form a double well for the adsorbed Sn atoms. The calculated energy barrier is close to the E_a range suitable for the observation of the thermally activated dynamical fluctuations in STM (0.13 – 0.15 eV at 80 K). Therefore, we suggest that an additional adsorbed Sn atom should flip between two traps of the double well at 80 K. The irregular bright spots visible on the lower terrace near the step edge in the σ map (Fig. 6(a)) originate, most probably, from the random Sn atoms trapped in the double wells. Note that there is a good correspondence between the positions of double wells along the step edge (Fig. 7, between edgemost Sn adatoms on the upper terrace) and the positions of bright spots in the measured σ map (Fig. 6(a)). This observation is an additional proof

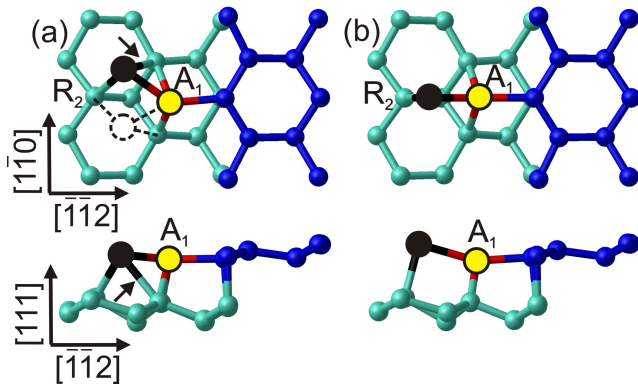


Figure 8. Atomic structures related to the $N = 3$ energy minima on the calculated PES. (a) Local minima configurations. (b) Saddle point configuration. Upper figures - top views, lower figures - corresponding side views. Cyan and blue circles are the Si atoms of the lower and upper terraces, respectively, the yellow circle is the A_1 Sn adatom at the step edge, black circle is the probe Sn (Si) adatom. The dashed circle shows the position of the probe adatom in the second local minima of the double well. The arrow highlights a weak bond between the probe adatom and the Si substrate.

of the developed step model and proposed interpretation of the experimental data.

The atomic configuration related to the PES energy minima $N = 3$ in the double well is shown in Fig. 8(a). According to this configuration, the adsorbed probe Sn atom is three-fold coordinated. The first bond is connected to the R_2 Si rest atom on the (111) terrace, the second bond is connected to the A_1 Sn adatom of the Sn atomic chain. The third bond (marked with an arrow) shares its connection to the substrate Si atom with the A_1 Sn adatom. The bond length between two Sn atoms is 2.95 Å, being very close to the calculated bond length in bulk α -phase Sn (2.91 Å). The bond lengths between the A_1 Sn adatom and Si substrate are 2.76 Å, 2.72 Å, 3.02 Å, while, for the probe Sn atom, they are 2.82 Å and 3.06 Å. The longest and, therefore, weakened Sn-Si bonds of about 3 Å in each group are connected to the same five-fold coordinated (overcoordinated) Si substrate atom. When the probe Sn atom is in its saddle position, as shown in Fig. 8(b), the weak bond between this atom and the overcoordinated substrate Si atom is

broken. The height change when moving the probe Sn atom from the position of energy minima to the saddle point is 0.57 Å.

For the sake of completeness, we also calculated PES for the probe Si atom on the stepped $\text{Si}(111) - \sqrt{3} \times \sqrt{3}$ -Sn surface to check if the observed fluctuations of tunneling current in STM can be caused by trapped Si atoms. We found that the positions of energy maxima and minima on PES are very similar to the ones observed for the probe Sn atom. This is explained by the same number of valence electrons in Si and Sn atoms. However, the values of calculated local energy minima, in case of the probe Si atom, are different. It is shown in Tab. I that the global minimum for the probe Si atom is on the $N = 8$ site, which is on the upper terrace just behind the A_1 adatom (Fig. 7). This result suggests that, unlike Sn atoms, Si atoms must accumulate at the upper terrace edge and be stationary at 80 K. Since this was not observed in the experimental STM images of step edges (Figs. 1(a)-1(c)), then Si adatoms can be excluded.

IV. CONCLUSIONS

In summary, the structure of the single step and dynamics of adatoms on the $\text{Si}(111) - \sqrt{3} \times \sqrt{3}$ -Sn surface were investigated by LT-STM at 80 K and *ab initio* calculations. The atomic model of the $[11\bar{2}]$ single steps on the $\text{Si}(111) - \sqrt{3} \times \sqrt{3}$ -Sn surface was developed. The model contains Sn atomic chains along the step edges. The adatom dynamics was detected at the lower side of the step edge in STM at 80 K. The PES calculated using the developed step model reveals the presence of double wells at the lower side of the step edge acting as traps for adsorbed Sn atoms. The random Sn atoms trapped within the double wells and flipping between two stable states explain the fluctuating current detected in STM at 80 K.

ACKNOWLEDGMENTS

RAZ would like to thank the Novosibirsk State University for providing the computational resources. Cluster computations and paper writing were supported by the Russian Science Foundation (project no. 19-72-30023).

* zhachuk@gmail.com

¹ S. Wirths, D. Buca, and S. Mantl, *Prog. Cryst. Growth Charact. Mater.* **62**, 1 (2016).

² T. Maeda, W. Jevasuwan, H. Hattori, N. Uchida, S. Miura, M. Tanaka, N. D. M. Santos, A. Vantomme, J. P. Locquet, and R. R. Lieten, *Jpn. J. Appl. Phys.* **54**, 04DA07 (2015).

³ M. Oehme, D. Buca, K. Kosteci, S. Wirths, B. Holländer, E. Kasper, and J. Schulze, *J. Cryst. Growth.* **384**, 71 (2013).

⁴ K. Yu, D. L. Zhang, H. Cong, X. Zhang, Y. Zhao, B. W. Cheng, and C. B. Li, in *IEEE 13th Int. Conf. Gr. IV Photonics* (2016) p. 34.

⁵ A. E. Dolbak and B. Z. Olshanetsky, *Cent. Eur. J. Phys.* **6**, 634 (2008).

⁶ X. W. Lin, *J. Vac. Sci. Technol. B* **13**, 1805 (1995).

⁷ S. Iwanari and K. Takayanagi, *J. Cryst. Growth.* **119**, 229 (1992).

- ⁸ S. Iwanari, Y. Kimura, and K. Takayanagi, *J. Cryst. Growth* **119**, 241 (1992).
- ⁹ K. Takayanagi, Y. Tanishiro, S. Takahashi, and M. Takahashi, *Surf. Sci.* **164**, 367 (1985).
- ¹⁰ J. T. Ryu, T. Fujino, M. Katayama, Y. B. Kim, and K. Oura, *Appl. Surf. Sci.* **190**, 139 (2002).
- ¹¹ A. Charrier, R. Pérez, F. Thibaudau, J. M. Debever, J. Ortega, F. Flores, and J. M. Themlin, *Phys. Rev. B* **64**, 115407 (2001).
- ¹² J. Nogami, S. Park, and C. F. Quate, *J. Vac. Sci. Technol. A* **7**, 1919 (1989).
- ¹³ C. Törnevik, M. Göthelid, M. Hammar, U. O. Karlsson, N. G. Nilsson, S. A. Flodström, C. Wigren, and M. Östling, *Surf. Sci.* **314**, 179 (1994).
- ¹⁴ C. Törnevik, M. Hammar, N. G. Nilsson, and S. A. Flodström, *Phys. Rev. B* **44**, 13144 (1991).
- ¹⁵ P. E. J. Eriksson, J. R. Osiecki, K. Sakamoto, and R. I. G. Uhrberg, *Phys. Rev. B* **81**, 235410 (2010).
- ¹⁶ A. H. Levermann, P. B. Howes, K. A. Edwards, H. T. Anyele, C. C. Matthai, J. E. Macdonald, R. Feidenhans'l, L. Lottermoser, L. Seehofer, G. Falkenberg, and R. L. Johnson, *Appl. Surf. Sci.* **104–105**, 124 (1996).
- ¹⁷ T. Ichikawa and K. Cho, *Jpn. J. Appl. Phys.* **42**, 5239 (2003).
- ¹⁸ B. Ressel, C. D. Teodoro, G. Profeta, L. Ottaviano, V. Cháb, and K. C. Prince, *Surf. Sci.* **562**, 128 (2004).
- ¹⁹ A. V. Latyshev, A. B. Krasilnikov, and A. L. Aseev, *Appl. Surf. Sci.* **60–61**, 397 (1992).
- ²⁰ T. Kato, T. Takajyo, H. Tochiyama, and W. Shimada, *Jpn. J. Appl. Phys.* **39**, 4307 (2000).
- ²¹ K. Romanyuk, V. Cherepanov, and B. Voigtländer, *Phys. Rev. Lett.* **99**, 126103 (2007).
- ²² B. Voigtländer, *Surf. Sci. Rep.* **43**, 127 (2001).
- ²³ S. A. Teys, K. N. Romanyuk, and B. Z. Olshanetsky, *J. Cryst. Growth* **404**, 39 (2014).
- ²⁴ D. I. Rogilo, L. I. Fedina, S. S. Kosolobov, B. S. Ranguelov, and A. V. Latyshev, *Phys. Rev. Lett.* **111**, 036105 (2013).
- ²⁵ F. Ronci, S. Colonna, S. D. Thorpe, A. Cricenti, and G. LeLay, *Phys. Rev. Lett.* **95**, 156101 (2005).
- ²⁶ F. Ronci, S. Colonna, A. Cricenti, and G. LeLay, *Phys. Rev. Lett.* **99**, 166103 (2007).
- ²⁷ F. Ronci, S. Colonna, A. Cricenti, and G. LeLay, *J. Phys.: Condens. Matter* **22**, 264003 (2010).
- ²⁸ N. Troullier and J. L. Martins, *Phys. Rev. B* **43**, 1993 (1991).
- ²⁹ J. M. Soler, E. Artacho, J. D. Gale, A. García, J. Junquera, P. Ordejón, and D. Sánchez-Portal, *J. Phys.: Condens. Matter* **14**, 2745 (2002).
- ³⁰ J. P. Perdew, K. Burke, and M. Ernzerhof, *Phys. Rev. Lett.* **77**, 3865 (1996).
- ³¹ F. Flores, J. Ortega, R. Pérez, A. Charrier, F. Thibaudau, J. M. Debever, and J. M. Themlin, *Prog. Surf. Sci.* **67**, 299 (2001).
- ³² G. Profeta and E. Tosatti, *Phys. Rev. Lett.* **98**, 086401 (2007).
- ³³ S. Modesti, L. Petaccia, G. Ceballos, I. Vobornik, G. Panaccione, G. Rossi, L. Ottaviano, R. Larciprete, S. Lizzit, , and A. Goldoni, *Phys. Rev. Lett.* **98**, 126401 (2007).
- ³⁴ S. Schuwalow, D. Grieger, and F. Lechermann, *Phys. Rev. B* **82**, 035116 (2010).
- ³⁵ H. J. Monkhorst and J. D. Pack, *Phys. Rev. B* **13**, 5188 (1976).
- ³⁶ J. Tersoff and D. R. Hamann, *Phys. Rev. B* **31**, 805 (1985).
- ³⁷ W. Kohn and L. J. Sham, *Phys. Rev.* **140**, A1133 (1965).
- ³⁸ I. Horcas, R. Fernández, J. M. Gómez-Rodríguez, J. Colchero, J. Gómez-Herrero, and A. M. Baro, *Rev. Sci. Instrum.* **78**, 013705 (2007).
- ³⁹ C. Battaglia, P. Aebi, and S. C. Erwin, *Phys. Rev. B* **78**, 075409 (2008).
- ⁴⁰ J. Avila, A. Mascaraque, E. G. Michel, M. C. Asensio, G. LeLay, J. Ortega, R. Pérez, and F. Flores, *Phys. Rev. Lett.* **82**, 442 (1999).
- ⁴¹ P. Gori, F. Ronci, S. Colonna, A. Cricenti, O. Pulci, , and G. LeLay, *EPL* **85**, 66001 (2009).
- ⁴² C. M. Chang and C. M. Wei, *Phys. Rev. B* **67**, 033309 (2003).
- ⁴³ R. Zhachuk, B. Olshanetsky, J. Coutinho, and S. Pereira, *Phys. Rev. B* **81**, 165424 (2010).